EurJIC
European Journal of Inorganic Chemistry

Research Article
doi.org/10.1002/ejic.202200709

Chemistry Europe
European Chemical Societies Publishing

www.eurjic.org

Oxo-Bridged Zr Dimers as Well-defined Models of Oxygen Vacancies on ZrO_2

Erik J. Wimmer,[a] Sina V. Klostermann,[b] Mark Ringenberg,[c] Johannes Kästner,[b] and Deven P. Estes*[a]

While ZrO_2 is known to have a large effect on the activity and selectivity of the Cu/ZrO_2 catalyst for methanol synthesis, its role in this process is poorly understood. Surface defects such as oxygen vacancies could play a role in the strong metal-support interaction (SMSI) between Cu and ZrO_2. However, due to the complexity of the surfaces, the exact molecular nature of this interaction is not at present known. Here, we make well-defined models of both reduced and coordinatively unsaturated surface oxygen vacancies on ZrO_2 using the molecular precursor $[Cp_2ZrCl]_2(\mu^2\text{-}O)$ (**1**). Complex **1** can be reduced to form a complex (**2**) containing one Zr(III) center and a bridging hydride ligand (according to EPR and IR spectroscopy) derived from C–H activation of either thf or the Cp ring. Complex **2** reacts with CO_2 to largely produce CO, suggesting that surface defects with similar structures probably do not play a role in the industrial catalyst. Halide abstraction from complex **1** results in the Lewis acidic species **3**, which has similar Lewis acid properties to acidic defects on the ZrO_2 surface. Similarities of both of these model species to real surface oxygen vacancies and their role in the catalytic reaction are discussed.

Introduction

ZrO_2 is commonly used in heterogeneous catalysis as both a solid catalyst and support material for metal nanoparticles. It is especially well-known as a support for the popular methanol synthesis catalyst Cu/ZrO_2.[1] Such methanol synthesis catalysts are known to be sensitive to the identity of not only the metal but also the metal oxide used to support that catalyst. This has led to the idea that the Cu/ZrO_2 catalyst exhibits a strong metal support interaction (SMSI), suggesting that the true active site for catalysis consists of both Cu and Zr centers working in unison.[2] Such an SMSI has also been seen for the $Cu/ZnO/Al_2O_3$ catalyst system for methanol synthesis.[3] In this system, the SMSI is thought to be caused by formation of CuZn alloys on the Cu surface that lower the activation barrier of the catalyst. Such a CuZn alloy is the result of reduction of ZnO to give isolated Zn atoms on the CuZn alloy surface.[4]

The origin of the SMSI in the case of Cu/ZrO_2 is not fully understood but may indeed be related to one of two mechanisms: hydrogen spillover or interfacial hydride transfer (Figure 1). Bell and co-workers postulated that hydrogen spillover from Cu onto the metal oxide (transfer of protons and electrons) is responsible for the catalytically active sites.[5] In situ IR studies of Cu/ZrO_2 have shown that CO_2 reacts with ZrO_2 to produce a reservoir of surface carbonate species and that the reaction intermediates are bound to ZrO_2. Cu/ZrO_2 was also shown to catalyze H/D exchange into both surface formate groups as well as OH groups.[6] Additionally, metal dopants in the ZrO_2 phase become reduced under catalytic conditions.[7] These are all signs of hydrogen spillover from the metal surface

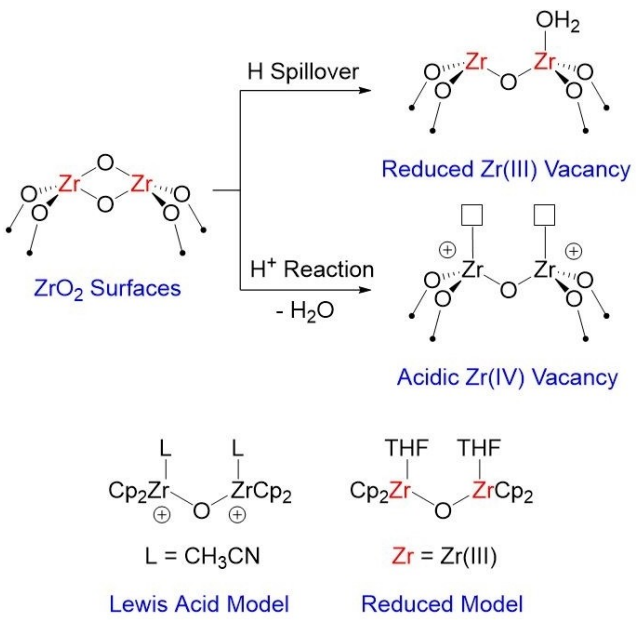

Figure 1. Oxygen vacancies on ZrO_2 surfaces and potential molecular analogues.

[a] E. J. Wimmer, Jun.-Prof. Dr. D. P. Estes
University of Stuttgart,
Institute of Technical Chemistry
Pfaffenwaldring 55, 70569 Stuttgart (Germany)
E-mail: deven.estes@itc.uni-stuttgart.de
[b] S. V. Klostermann, Prof. Dr. J. Kästner
University of Stuttgart,
Institute for Theoretical Chemistry
Pfaffenwaldring 55, 70569 Stuttgart (Germany)
[c] Dr. M. Ringenberg
Société Suisse des Explosifs
Fabrikstrasse 48, CH–3900 Brig (Switzerland)

Supporting information for this article is available on the WWW under https://doi.org/10.1002/ejic.202200709

Research Article
doi.org/10.1002/ejic.202200709

to the metal oxide.[8] In the spillover mechanism, the catalytically active species are located mostly on the metal oxide surface and the Cu metal acts as a $H^{\bullet}$ source, which it donates to the surface in a proton electron transfer (PET) reaction.[8b] This results in reduced metal sites and new OH bonds, eventually leading to loss of water from the surface. Therefore, the potential active sites in this reaction would be coordinatively unsaturated Zr(III) sites with nearby OH groups. However, such sites have never been observed directly during catalysis. Moreover, even if these sites were formed, it is not clear how they would react with CO_2 on a molecular level to produce formate or methoxy species.

Another theory is that the Lewis acid sites on the catalyst surface form active sites that can increase the rate of formate hydrogenation. Copéret et al. showed that while formate species are attached to the metal oxide surface they are hydrogenated by hydrides from a nearby Cu surface.[9] They postulated that the catalytic reaction occurs at the interface between Cu and ZrO_2 surfaces. This agrees with homogeneous catalytic reactions, in which added Lewis acids activate molecular catalysts for CO_2 hydrogenation to MeOH by activation of the formate intermediates.[10] However, this mechanism would limit the active sites to being within a few Å of the interface between Cu and ZrO_2.

Both the Lewis acid sites and the reduced centers postulated above would occur at oxygen vacancy defects. One potentially relevant surface defect on both tetragonal and monoclinic ZrO_2 are μ^2-O vacancies, created by removal of a doubly bridging oxide ligand from the surface (Figure 1).[11] Formation of oxygen vacancies on such surfaces (shown in Figure 1) involve the loss of μ^2-oxygen atoms either resulting in cationic oxygen vacancies that are strongly Lewis acidic or neutral oxygen vacancies consisting of Zr(III) sites. However, due to the complex nature of the surfaces in question, the reactivity of the defect sites under reaction conditions is not well understood. In order to clarify the role of such defect sites in the catalytic reactivity, it is desirable to make well-defined molecular models of both types of oxygen defects (both Lewis acidic and neutral (Zr(III)) defects) and characterize their structures and reactivities with CO_2 using coordination chemistry methods. In this paper, we generate well-defined models of ZrO_2 oxygen vacancies and test their reactivity, both as Lewis acids and as redox centers. We accomplish this by using the $[Cp_2ZrCl]_2(\mu^2\text{-O})$ (**1**) skeleton to simulate the bridging μ^2-oxo structural motif of the ZrO_2 surface atoms (shown in Figure 1). We show that models of both the cationic and the reduced oxygen vacancies can be generated from this species and that they show interesting reactivity that may be relevant to CO_2 hydrogenation.

Results

Reduction of Zr oxo-bridged dimers

Reduction of group 4 metal halides is known to produce M(III) species.[12] Therefore, synthesis of our model compounds could be possible starting with the well-known dimeric oxo-bridged Zr complex $(Cp_2ZrCl)_2(\mu^2\text{-O})$ **1**. The CV of **1** in THF (Figure S1) exhibits an irreversible reduction peak at −2.3 V vs. $Ag/AgNO_3$ (−2.21 V vs. Fc). We therefore set out to chemically reduce the oxo-bridged Zr dimer **1** with appropriately strong reductants and produce molecular models of reduced oxygen vacancies. Reaction of **1** with Mg metal and a small amount of I_2 at 50 °C in THF for 2 h resulted in a dark purplish-red solution indicative of a reduced Zr species. This reaction seems to be sensitive to many factors including reductant, solvent, and additives. We attempted this reaction with many different reductants including Na, K, KC_8, NaH, nBuLi, decamethylcobaltocene, and a series of organosilicon-based reductants,[13] none of which resulted in reduction. Na(1-Me–naphthalide) and Mg were the only two reducing agents capable of reducing complex **1** in our hands. The reaction with Mg requires the addition of I_2 in order to proceed. This results in an orange solution that becomes colorless over ca. 15 min after which the deep purplish-red color of the reduced Zr complex begins to form. If the Mg is instead pre-treated with I_2 and complex **1** added after the solution turns colorless the reaction also does not proceed. Additionally, coordinating solvents such as THF and dioxane were optimal for the reaction. While we were not able to isolate complex **2** in pure form, it can be isolated as an adduct with $MgCl_2$ by removal of solvent and washing with hexane to give a dark purple solid that reacts very rapidly with air. The reason for the sensitivity of the reaction to certain solvents and reductants is not at this time clear, but may be due to a more complex electron transfer mechanism (e.g. radical chains[14] or C–H activations, see below).

Characterization revealed that indeed the reduction did result in a Zr(III) complex. The ^{1}H NMR spectra (Figure S2–3) showed broadened signals due to the Cp rings (5.1–6.5 ppm) and coordinated THF (3.6 and 1.4 ppm). Measurement of the magnetic susceptibility by Evans method[15] gave a magnetic moment of 1.32 μ_B (Table S1), indicative of a single reduced Zr(III) center in the dimer. EPR spectroscopy (Figure 2) showed an isotropic doublet at room temperature with $g = 1.987$ and $A = 19.5$ MHz (6.9 G) with a smaller signal at $g = 1.979$. The same EPR spectrum is observed regardless of which reductant is used. The g value and the coupling constant of the doublet are reminiscent of Zr(III)–H species from the literature, which have g values of 1.985–1.987 and A_H values of 5.6–7.0 G.[16]) The IR spectrum (KBr pellet, Figure 2) showed no peaks consistent with a terminal Zr–H bond (expected between 1550–1700 cm^{-1}) but instead showed a new broad intense peak centered around 1342 cm^{-1} tailing down to 1200 cm^{-1} that disappears upon oxidation of the complex (Figures S5–6). This peak most likely consists of several overlapping signals but would be consistent with other Zr–H–Zr bonds known in the literature (1355 cm^{-1}).[17] DFT simulations of the IR spectrum of proposed complex **2** (Figure S12) showed a Zr–H–Zr stretching frequency at 1160 cm^{-1} (Figure S13), which is somewhat lower than both our observation and previous reports. Given that the broad peak tails down to about 1200 cm^{-1}, the true Zr–H–Zr stretching mode may appear at the lower end of this broad peak and would therefore be consistent with the DFT

Research Article
doi.org/10.1002/ejic.202200709

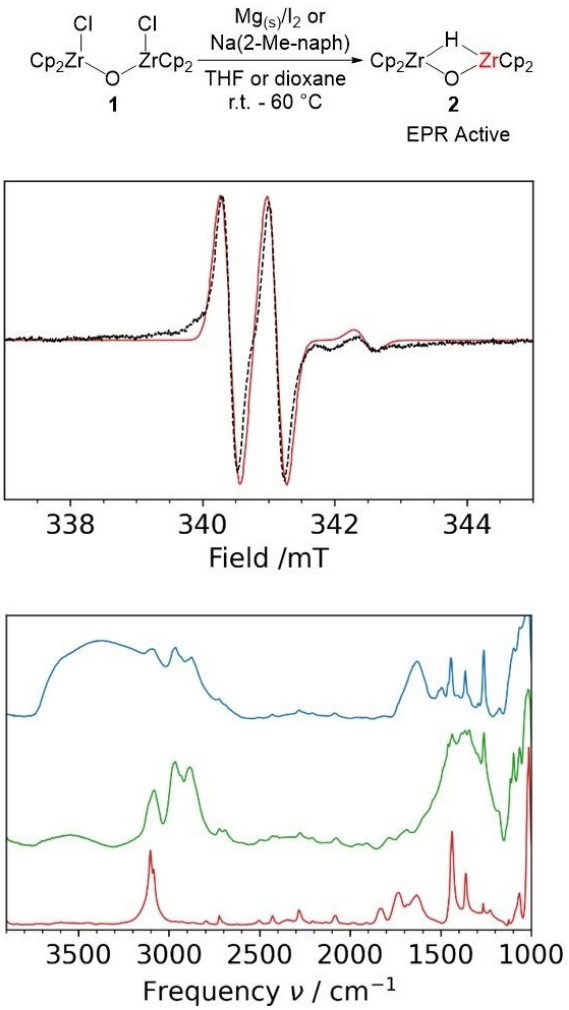

Figure 2. (top) Reduction of complex **1** with various chemical reductants. (middle) EPR spectrum of reduced complex **2** (experiment (black), simulation (red)) and (bottom) IR-spectroscopy of **1** (red), reduced (hydride) **2** (green) and reoxidized (blue).

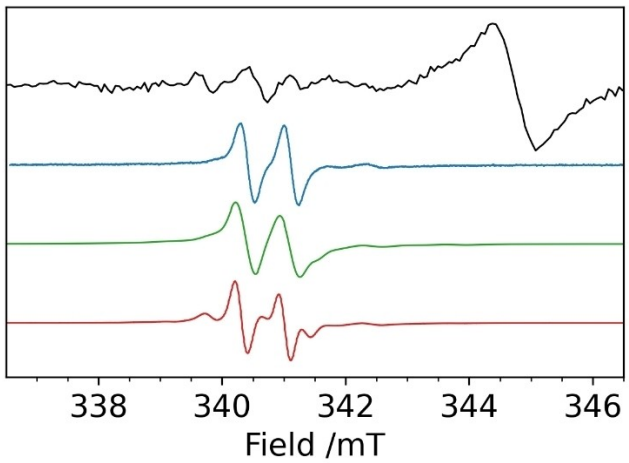

Figure 3. EPR spectra of electrochemically reduced **1** after 10 min reaction time (black), 6.5 mM solution of **2** (blue), in situ reduction of **1** using Mg/I_2 in thf (green), and **1** reduced in situ by Mg/I_2 in thf-d_8 (red).

calculations. Efforts to crystallize **2** were unsuccessful and, indeed, it was not possible to remove certain amounts of Mg or Na cations, as seen by elemental analysis. The Mg or THF present in the complex could also result in a perturbation of the vibrational frequency in the form of vibrational mixing or slight structural perturbations, resulting in a shift of the Zr–H–Zr stretching frequency from that predicted by DFT. Based on the spectroscopic characterization, we propose a structure consisting of one Zr(III) center and one Zr(IV) center connected by a bridging hydride.

We then set about to understand how this structure could form during the reduction step. The first aspect we want to understand is where does the H come from to make the bridging hydride? We carried out EPR-spectroelectrochemistry to look for the intermediate Zr(III)/Zr(III) dimer expected upon reduction (Figure 3). Electrolysis at < -2.2 V directly in the EPR cavity resulted in an EPR spectrum with a new signal at $g = 1.965$. The origin of this signal is unclear, but does not match the EPR spectrum expected for a Zr(III)/Zr(III) dimer with a triplet ground state, which should be similar to the known EPR spectrum of its Ti congener.[18] Most likely, this peak represents the singly reduced Zr(III)/Zr(IV) intermediate. After a matter of ca. 5 min, this signal began to give way to the doublet belonging to **2**. Monitoring the reaction of Mg/I_2 in thf showed only the isotropic doublet attributed to **2**, regardless of reaction time. However, the EPR spectrum of the reaction of **1** with Mg/I_2 in thf-d_8 showed both the same isotropic doublet of **2** and a 1:1:1 triplet with identical g-value (Figure 3 (red)). This triplet can be attributed to **2**-d_1, and must be the result of C–H activation of the solvent thf-d_8. However, given that not all **2** becomes labelled when running the reaction in 100% thf-d_8, it is also possible that some bridging hydride ligand is derived from C–H activation of the Cp rings.

Activation of the C–H bonds on Cp rings has previously been observed for Cp_2Zr and other highly-reduced early transition metal Cp complexes, in some cases even forming bridging H species.[19] C–H activation of the solvent may be the reason for the solvent specificity of the reaction (the weak C–H bonds of thf and dioxane can be activated by the complex).

DFT calculations were done to evaluate the energetic feasibility of this C–H activation step. Full details are included in the Supporting Information (Figures S8–S13). As depicted in Figure 4, Struc1 is preferred over the agostic Struc2 by just $\Delta E = 24.2\ kJ\,mol^{-1}$. To get to the H-activated Struc3 another energy barrier has to be overcome ($\Delta E_{Struc2\text{-}TS} = 51.0\ kJ\,mol^{-1}$). A total activation energy of $E_A = 75.2$ kJ/mol is needed for the C–H activation. This barrier is consistent with our reaction taking place at slightly elevated temperatures (336 K).

We next reacted compound **2** with CO_2 in order to see what effect such sites could have on the selectivity of CO_2 hydrogenation on surfaces. Indeed, when electrochemical reduction of **1** is performed by CV under a CO_2 atmosphere (Figure S1), the current of the reduction wave (giving **2**) is somewhat increased (by ca. 20%) suggesting that **2** does react with CO_2.

Research Article
doi.org/10.1002/ejic.202200709

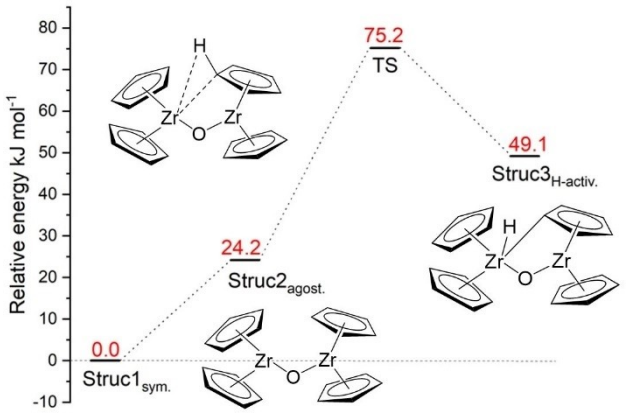

Figure 4. Energy diagram for C–H activation of compound **2** with transition state TS.

Exposure of a solution of **2** to a CO_2 atmosphere causes a color change from purplish-red to yellow at room temperature over ca. 3 h. During the reaction, gas formation was observed from the solution. After the reaction had ended, the gas phase was analyzed by GC analysis (Figure S7) and found to contain not only CO_2 but also CO. CO was observed regardless of the reductant used. Similar reactions of CO_2 with low valent group 4 metals have also been shown to produce CO.[20]

We then attempted the reaction catalytically using excess chemical reductant (results shown in Table 1). This resulted in very low catalytic turnover (TON = 4 for Mg, TON = 2 for Na[2-Me–naphthalide]) giving CO. In an attempt to shift the selectivity toward formate products, we added H^+ sources such as EtOH and phenol. However, this resulted in the preferential formation of H_2 and merely reduced the CO yield. For reactions with both acid and reductant present, the H_2 produced was not quantified. However, from this we can surmise, that Zr(III) centers created on the surface of the Cu/ZrO_2 catalyst are subject to reoxidation by the water produced during the hydrogenation of CO_2.

Lewis acidity of cationic Zr oxo-bridged dimers

We next wanted to understand how the Lewis acidity of coordinatively unsaturated and potentially cationic oxygen vacancies on surfaces could influence the reactivity of the surface toward CO_2 hydrogenation to methanol. Therefore, we set about to create model species of cationic oxygen vacancies.

Table 1. Reactivity of **2** with CO_2 using various reductants and acids.

No	reductant	H^+ source	t and T	Main Product	TON
1	Mg	–	90 min 60 °C	CO	4.0(6)
2	Mg	EtOH	90 min 60 °C	CO/H_2	2.4
3	Mg	Phenol	90 min 60 °C	CO/H_2	1.8
4	Na[2-Me–Naph]	–	90 min r.t.	CO	1.8(2)
5	Na[2-Me–Naph]	EtOH	90 min r.t.	CO/H_2	1.0
6	Na[2-Me–Naph]	Phenol	90 min r.t.	CO/H_2	1.0

We first reacted the dimer **1** with $Ag[BF_4]$ in various solvents. In thf, addition of $Ag[BF_4]$ resulted in AgCl precipitation followed by thickening of the solution forming a highly viscous intractible mixture indicative of polymerization of thf. This is known to occur upon exposure of thf to strong Lewis acids.[21] However, reaction of $Ag[BF_4]$ (2 equiv) with **1** in CH_2Cl_2 containing a few drops of CH_3CN produces a stable cationic Zr product (NMR spectrum shown in Figure S4). The IR spectrum (Figure 5) of the soluble product of this reaction exhibits two new bands at 2291 cm^{-1} and 2320 cm^{-1} attributable to ν_{CN} of CH_3CN adsorbed on Lewis acid sites. This is comparable to the results of acetonitrile adsorption on ZrO_2 giving $\nu_{CN} = 2283\ cm^{-1}$ and 2314 cm^{-1}.[22] This suggests that the strength of the Lewis acid sites of the $Zr(NCCH_3)$ complex **3** is similar to those of oxygen vacancies on the ZrO_2 surface, showing they are good models of the surface Lewis acid sites in terms of reactivity.

Discussion: Comparison to Vacancies on ZrO_2

We next wanted to understand the relevance of our findings to real oxygen vacancies that could be relevant to the catalytic reaction. Formation of oxygen vacancies during catalysis has been observed spectroscopically. For an inverse catalyst with a small amount of ZrO_2 supported on a Cu surface, in situ XPS measurements showed that oxygen vacancies did indeed form on amorphous ZrO_2 during CO_2 hydrogenation.[23] However, the nature of these sites could not be confirmed spectroscopically, due to inhomogeneities in the ZrO_2 structure on the Cu surface. For this reason, molecular model studies are ideal for connecting reactivity with potential structural elements of the metal oxide surfaces. However, some effects such as electron transport in bulk media and the steric properties of surfaces are difficult to mimic with model systems.

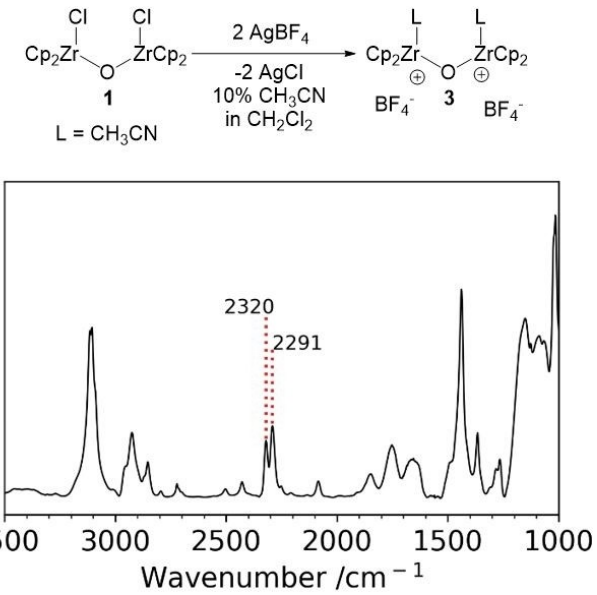

Figure 5. Synthesis and IR spectrum of compound **3** with acetonitrile CN stretching bands marked in red.

Research Article
doi.org/10.1002/ejic.202200709

In order to understand how the chemistry of **2** and **3** relate to that of a true ZrO_2 surface, we compared the spectroscopic signatures of our model species to those of true surface vacancies. We measured the UV-Vis spectrum of species **2** both before and after oxidation and of complex **3** (Figure 6). Compound **2** showed absorptions at 410, 513, and 660 nm, as a result of the Zr(III) center, with high absorbances in the UV region due to the Cp rings. In comparison, Evans and coworkers prepared ZrO_2 samples with varying proportions of surface defect sites and found that the UV-Vis spectrum was dependent on the amount of defect sites in the sample. In particular, they showed that high amounts of defects resulted in increased absorption into the visible region centered around 540 nm, similar to what we and many others have observed for Zr(III) species.[24] In contrast, complex **3** showed no features in the visible region but an increased intensity into the UV. This suggests that discoloration of ZrO_2 upon reduction at high temperatures is not due to formation of cationic oxygen vacancies but rather of reduced oxygen vacancies (Zr(III)) or of injection of electrons into the conduction band of bulk ZrO_2.

EPR spectroscopy of the oxygen defects on ZrO_2 poses an interesting question for the chemist. Indeed, after heating a sample of monoclinic – ZrO_2 under vacuum (or in the presence of H_2) at 500 °C, a singlet appears in the X-band EPR spectrum at $g = 2.0026$ and a smaller signal appearing at $g = 2.0065$. These signals have been observed before and are typically attributed to so-called "trapped electrons".[25] However, no structural description of these electrons have ever been given in the literature, to our knowledge. Its proximity to the free electron value ($g_e = 2.0023$) leads us to believe that it could either be attributed to an oxygen based radical or to a free electron delocalized in the bulk material. Similar EPR signals have been assigned for TiO_2, but are certainly not consistent with localized Zr(III) or Ti(III) sites. Further discussion of the chemical nature of such trapped electrons is beyond the scope of this publication.

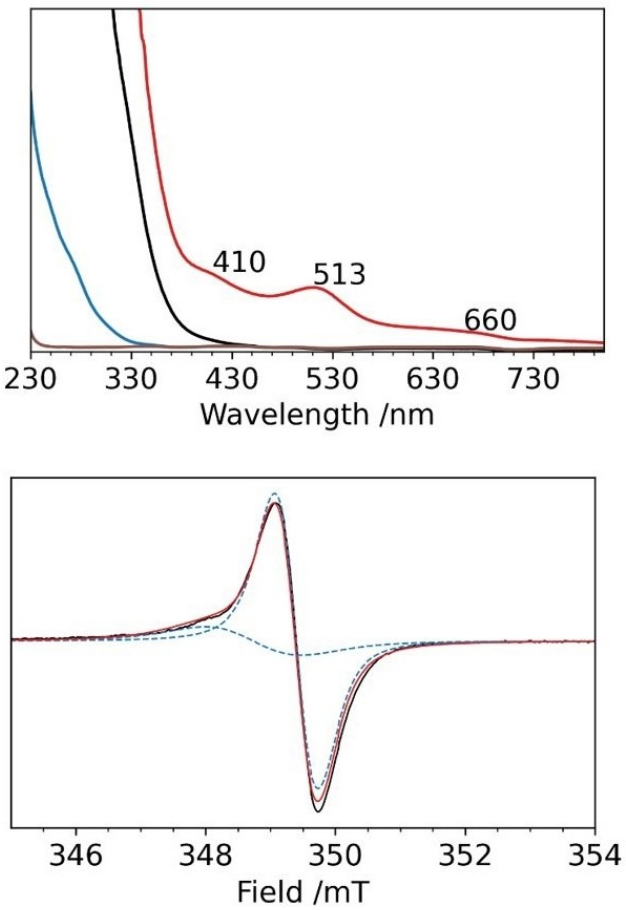

Figure 6. (top) UV-Vis spectrum of **2** (red), oxidized **2** (black), **3** (blue), and blank (brown). (bottom) EPR spectrum of ZrO_2 treated at high temperature (black) along with simulation (red) and individually fitted components (dotted blue lines).

The reactivity of the reduced molecular model that we have made here suggests that Zr(III)–H centers with similar structural and spectroscopic features on the catalyst surface would be more selective for CO production than for methanol production. However, since a model study can only connect reactivity with a particular structure, we cannot use this as hard proof that such Zr(III) species do not play a role in the catalytically active site. Indeed, variations in the structure of Zr(III) related oxygen vacancies and even proximity of Zr(III) sites to OH centers could change the selectivity in favor of methanol production. Therefore, more work on the operating catalyst is needed to understand the structure of any reduced Zr sites and oxygen vacancies formed during catalysis.

Given the propensity of Zr(III) sites for production of CO from CO_2, the activation of CO_2 by Lewis acidic oxygen vacancies on ZrO_2 becomes an attractive explanation for the high methanol selectivity in these systems. The fact that the ν_{CN} bands of acetonitrile are similar to those observed on ZrO_2 surfaces, suggests that complex **3** is a good model for the Lewis acidic centers on the surface. Indeed, there is a connection between the activity of Cu based catalysts for methanol synthesis and the Lewis acidity of the metal oxide used as a support. In one compelling literature example, overlayers of various Lewis acidic metal oxides were synthesized on porous Al_2O_3 and their Lewis acidity was measured using probe molecules. When Cu nanoparticles of uniform size were dispersed on these surfaces, they found a direct correlation between the activation energy for methanol formation and the Lewis acidity of the oxide overlayer.[26] This would suggest that the Lewis acidity of cationic oxygen vacancies could be pivotal for the reactivity of the Cu/ZrO_2 catalyst.

It has also long been known that Cu/ZrO_2 made with tetragonal ZrO_2 is more active than with monoclinic ZrO_2.[27] Periodic DFT calculations of the structure of ZrO_2 nanoparticles show that monoclinic surfaces consist of about 45% of the (−111) termination while tetragonal surfaces are composed of 49% of the (111) facet.[28] Our complex **3** is missing one O atom from its coordination sphere and is thus a reasonable model of a μ^2 bridging oxygen vacancy. If we compare these two crystal facets, about 33% of the oxygen atoms on the t-ZrO_2 (111) facet are μ^2 bridging oxides, while only 14% of the oxygen atoms on m-ZrO_2 (−111) are μ^2 bridging. This would indeed suggest that the more active catalyst (Cu/t-ZrO_2) is the one with

Research Article
doi.org/10.1002/ejic.202200709

a greater density of doubly bridging oxygen atoms and therefore has a greater propensity for forming Lewis acidic bridging oxygen vacancies. Thus, it is a reasonable proposal that Lewis acidic bridging oxygen vacancies play a role in the desirable catalytic activity of the Cu/ZrO_2 system. Just as above, more studies on the working catalyst, in particular operando spectroscopic studies, will be necessary to determine the structure of vacancies formed during catalysis.

Conclusions

We synthesized oxo-bridged dinuclear Zr complexes as models of both cationic and neutral oxygen vacancies on ZrO_2 surfaces and compared their reactivity for CO_2 reduction. Complex **1** reacts with selected strong reductants to form the reduced bridging hydride complex **2**, formed by C–H activation of the Cp ring and solvent, as shown by EPR and IR spectroscopies and by DFT calculations. This reduced hydridic species reacts with CO_2 to exclusively form CO and reacts with acids to form H_2, suggesting that involvement of such Zr(III) containing surface defects in selective CO_2 hydrogenation to methanol is unlikely. Treatment of complex **1** with $Ag[BF_4]$ forms the cationic complex **3**. Cationic complex **3** binds strongly to coordinating solvents such as acetonitrile. Comparison of the ν_{CN} of **3** vs. ZrO_2 surfaces suggests that they have very similar Lewis acid strengths. Comparison of the UV-Vis and EPR spectra of **2** with reduced ZrO_2 surfaces suggests that surfaces with high vacancy proportions have similar UV-Vis spectra but somewhat different EPR spectra. This suggests that EPR active vacancies are either oxygen based or are delocalized across the material and cannot be assigned as pure Zr(III) species. However, surfaces that have more doubly bridging oxygen species make more active catalysts, meaning that such cationic defect sites could play a significant role in the active site of Cu/ZrO_2.

Experimental Section

General: All materials and chemicals were used as received from the manufacturer unless otherwise stated. Syntheses and reactions were carried out under argon atmosphere using standard Schlenk and glovebox techniques. Glassware was flame dried and/or stored in an oven (120 °C) prior to use. Solvents were dried and distilled after the recommendation of D. F. Shriver[29] and stored over molecular sieves under argon. Tetrahydrofuran (Sigma-Aldrich, 99.9%, stabilizer free, Catalog number 34865) and dioxane (Sigma-Aldrich, 99.9%, stabilizer free, catalog number 296309) were dried over sodium–benzophenone ketyl and distilled prior to use. Diethyl ether was dried over molecular sieves. Acetonitrile (VWR, catalog number 20070.291, >99%), dichloromethane (Friedrich Scharr KG, >99.8%), and n-hexane (Bernd Kraft GmbH, >99.8%) were sparged with argon to remove residual air, dried by passage through an activated alumina column, and stored under Ar over activated molecular sieves. Deuterated solvents were obtained from Eurisotop (catalog numbers: D149FE (thf-d_8), D001FE (C_6D_6)) were dried over molecular sieves, degassed by three freeze-pump-thaw cycles, and stored in a N_2 glove box. Gases were treated to remove water and oxygen before use. Carbon dioxide gas was degassed by three freeze-pump-thaw cycles and stored over molecular sieves in a vacuum flask. Hydrogen gas was purified by passing it through a column of high surface area copper and a liquid nitrogen cooling trap to remove oxygen and water and stored over molecular sieves in a vacuum flask. The following chemicals were purchased from the listed chemical suppliers and used as received. Magnesium turnings (Sigma Aldrich, catalog number 200905, 98%), sodium metal (Merck, catalog number 71172, 99.8%), 2-methylnaphthalene (Sigma-aldrich, catalog number M57006, 97%), silver tetrafluoroborate (STREM, catalog number MFCD00003408, 99%), Cp_2ZrCl_2 (Sigma Aldrich, catalog number 196215, 98%), aniline (Merck, catalog number 242284, 99.5%).

IR spectra were measured using a Nicolet 6700 IR spectrometer. Air sensitive solids were measured in transmission mode in a home-made glass sample holder with CaF_2 windows as KBr pellets using pre-dried KBr. Typical KBr pellets were made by mixing ca. 2 mg of Zr complex with ca. 50 mg of KBr in a mortar and pestle in an argon glove box before pressing into a 7 mm diameter pellet at 2 tons pressure. Air stable samples were measured in ATR mode using a diamond crystal ATR attachment. EPR spectra were measured on one of two Bruker cw X-band EMX spectrometers at room temperature. EPR simulation was performed using the EasySpin toolbox for MATLAB.[30] UV-Vis spectra were measured on a Cary 60 UV-Vis spectrometer in toluene solvent with a path length of 1 mm. Liquid state NMR spectra were measured on either a 300 or 400 MHz Bruker AVIII spectrometer. Evans method measurements were conducted versus a sealed capillary of C_6D_6 and were corrected for the diamagnetic components according to the known structure of precursor **1** and the elemental analysis.[31]

Synthesis of 2: Mg as reductant: $[Cp_2ZrCl]_2$-μ^2-O (**1**) (500 mg, 0.94 mmol), prepared according the the literature procedure,[32] was dissolved in thf (20 ml). Magnesium (250 mg, 10.3 mmol) was added and stirred while heating to 50 °C. An iodine crystal (ca. 2–5 mg) was added upon which the solution turned orange. After 15 minutes the iodine color faded and the solution slowly became dark purplish-red (red wine color) over the course of 2 h. The solution was cooled to −78 °C by immersion in a dry ice/acetone bath for 20 min, filtered at low temperature, and the solvent removed under vacuum. After drying under vacuum (10^{-3} mbar) a dark purple solid was obtained (499 mg, ca. 0.48 mmol, ca. 50% yield). Despite many attempts, it was not possible to free the deep purple powder of Mg impurities.

EA: Anal. calcd for $C_{36}H_{53}Cl_6Mg_3O_5Zr_2$: C 41.82, H 5.17 found: C 42.04, H 5.19, **ICP**: 2 Mg/**1**, **IR** (KBr): 3080 (m), 2964 (m), 2885 (m), 1437 (m), 1342 (m, Zr–H–Zr), 1261 (m), 1097 (w), 1016 (s), **Evans method**: 1.32 μ_B, **EPR**: g-value: 1.987)

NaNaph as reductant: Sodium 2-methylnaphthalide was synthesized by adding sodium (2 equiv. vs. **1**) to a solution of 2-methylnaphthalene in thf. After 6–18 h all sodium had reacted producing and a dark green solution. Upon addition of **1**, the solution turned dark brown. The crude product is washed with n-hexane (3×2 ml). Drying under vacuum gave a dark brown-purple solid. The characterization from this method was similar to above.

Catalytic reaction of 2 with CO_2: Reaction given above was done under a) Argon and b) CO_2 atmosphere. If the reaction was done under argon the atomosphere was exchanged.

Addition of ethanol/phenol lead to discoloration and decomposition. Gas phase analysis of product mixture (CO, H_2) was performed by GC using an Agilent 7890 A GC equipped with a thermal conductivity detector. CO_2 was separated from the gas mixture by injection first into a PlotQ column. After this, the remaining product gases were injected into an HP-Molesieve capillary column allowing for analysis of the product gases. ^{1}H NMR was used to analyze the

liquid phase for products such as formate/formic acid, methanol, or other liquid phase products. No liquid phase products were ever observed during these studies.

Synthesis of 3: Compound **1** (30 mg, 0.056 mmol) was dissolved in CH_2Cl_2/CH_3CN. $AgBF_4$ (21.8 mg, 0.112 mmol) was added and immediately a white solid precipitated. The mixture was filtered to remove AgCl, the solvent removed and dried shortly under vacuum to yield **3** as a white powder (39 mg (0.056 mmol, $>99\%$).

NMR: ^{1}H NMR (400 MHz, Benzene-d_6): $\delta = 5.93$ (s, 20H (Cp)). **EA**: $C_{24}H_{26}B_2F_8N_2OZr_2 \cdot H_2O$: C 39.35, H 3.85, N 3.82 found: C 39.29, H 3.57, N 3.98, **IR**: 3114 (s, Cp–H), 2925 (m, $-CH_3$), 2854 (m, $-CH_3$), 2320 (m, CN-Fermi resonance), 2291 (m, CN), 1439 (s, Cp ring stretch).

Preparation of ZrO_2 Surface: Monoclinic ZrO_2 was heated to 500 °C in a glass reactor under high vacuum (10^{-5} mbar). After this time, the ZrO_2 was slightly discolored and exhibited the EPR spectrum seen in Figure 6. This material was allowed to cool under dynamic vacuum and stored in sealed glass tubes in an Ar glovebox.

Electrochemistry Experiments: CV measurements were conducted using a glassy carbon working electrode, Pt wire counter electrode, vs. a $Ag/AgNO_3$ reference electrode in thf solution containing 0.1 M $NBu_4[B(C_8H_3F_6)_4]$ electrolyte under 1 atm of either Ar or CO_2. The measurements were referenced to ferrocene (internal standard) added after the experiments.

Spectroelectrochemistry experiments: Complex 1 (0.1 M in thf) was dissolved in a 0.2 M solution of tetrabutylammonium tetrafluoroborate. This was placed in a quartz EPR tube outfitted with a Pt wire working electrode and Pt wire counter electrode. The voltage from a power supply was increased until a current of ca. 150 μA was registered, (approx. 1.8 V unreferenced) for 20–30 min. EPR spectra were measured at room temperature over varying time intervals during the reaction.

Computational Details: DFT calculations were carried out using the Turbomole V7.4 software package (TURBOMOLE V7.4 2019, a development of University of Karlsruhe and Forschungszentrum Karlsruhe GmbH, 1989–2007, TURBOMOLE GmbH, since 2007; available from http://www.turbomole.com and the molecular Amsterdam Densitiy Functional programm (Version 2022.103) (only for IR calculations).[33] The initial geometries were optimized on the PBE–D3(BJ)/def2-SVP level.[34] On these optimized geometries, single-point energies were calculated on the M06/def2-TZVPD level.[35] All relative energies include zero-point vibrational energies (ZPE) and are related to the energy of Struc1. Transition state search was performed with the dimer method[36] on the PBE–D3(BJ)/def2-SVP level of theory. All calculations were performed including the solvent tetrahydrofuran (THF), using the conductor-like screening model (COSMO)[37] with a dielectric constant of $\varepsilon = 7.6$.

Acknowledgements

The authors would like to sincerely thank the German research foundation (DFG Project numbers 444948747 and 358283783-SFB1333/2) as well as the University of Stuttgart for generous financial support for this work. The authors also acknowledge support by the state of Baden-Württemberg through bwHPC and the German Research Foundation (DFG) through grant no INST 40/575-1 FUGG (JUSTUS 2 cluster). Open Access funding enabled and organized by Projekt DEAL.

Conflict of Interest

The authors declare no conflict of interest.

Data Availability Statement

The data that support the findings of this study are openly available in DARUS at https://doi.org/10.18419/darus-3259, reference number 3259.

Keywords: CO_2 reduction · hydrides · lewis acid model · oxygen vacancy · zirconium

[1] a) T. Witoon, J. Chalorngtham, P. Dumrongbunditkul, M. Chareonpanich, J. Limtrakul, *Chem. Eng. J.* **2016**, *293*, 327–336; b) W. Herzog, *Angew. Chem. Int. Ed. Engl.* **1972**, *11*, 649.
[2] a) C. Wu, L. Lin, J. Liu, J. Zhang, F. Zhang, T. Zhou, N. Rui, S. Yao, Y. Deng, F. Yang, W. Xu, J. Luo, Y. Zhao, B. Yan, X.-D. Wen, J. A. Rodriguez, D. Ma, *Nat. Commun.* **2020**, *11*, 5767; b) J. Schumann, M. Eichelbaum, T. Lunkenbein, N. Thomas, M. C. Álvarez Galván, R. Schlögl, M. Behrens, *ACS Catal.* **2015**, *5*, 3260–3270.
[3] a) M. Zabilskiy, V. L. Sushkevich, D. Palagin, M. A. Newton, F. Krumeich, J. A. van Bokhoven, *Nat. Commun.* **2020**, *11*, 2409; b) M. Behrens, F. Studt, I. Kasatkin, S. Kühl, M. Hävecker, F. Abild-Pedersen, S. Zander, F. Girgsdies, P. Kurr, B.-L. Kniep, M. Tovar, R. W. Fischer, J. K. Nørskov, R. Schlögl, *Science* **2012**, *336*, 893–897.
[4] E. Frei, A. Gaur, H. Lichtenberg, L. Zwiener, M. Scherzer, F. Girgsdies, T. Lunkenbein, R. Schlögl, *ChemCatChem* **2020**, *12*, 4029–4033.
[5] a) K. Pokrovski, K. T. Jung, A. T. Bell, *Langmuir* **2001**, *17*, 4297–4303; b) T. J. Keskitalo, M. K. V. Niemelä, A. O. I. Krause, *Langmuir* **2007**, *23*, 7612–7619.
[6] K.-D. Jung, A. T. Bell, *J. Catal.* **2000**, *193*, 207–223.
[7] a) Tobin, C. Schilke, I. A. Fisher, A. T. Bell, *Catal. Lett.* **1998**, 105–111; b) K. Pokrovski, A. Bell, *J. Catal.* **2006**, *241*, 276–286.
[8] a) W. C. Conner, J. L. Falconer, *Chem. Rev.* **1995**, *95*, 759–788; b) R. Prins, *Chem. Rev.* **2012**, *112*, 2714–2738.
[9] K. Larmier, W.-C. Liao, S. Tada, E. Lam, R. Verel, A. Bansode, A. Urakawa, A. Comas-Vives, C. Copéret, *Angew. Chem. Int. Ed. Engl.* **2017**, *56*, 2318–2323.
[10] a) J. Klankermayer, S. Wesselbaum, K. Beydoun, W. Leitner, *Angew. Chem. Int. Ed.* **2016**, *55*, 7296–7343; *Angew. Chem.* **2016**, *128*, 7416–7467; b) K. Thenert, K. Beydoun, J. Wiesenthal, W. Leitner, J. Klankermayer, *Angew. Chem. Int. Ed.* **2016**, *55*, 12266–12269; *Angew. Chem.* **2016**, *128*, 12454–12457; c) S. Wesselbaum, T. vom Stein, J. Klankermayer, W. Leitner, *Angew. Chem. Int. Ed.* **2012**, *51*, 7499–7502; *Angew. Chem.* **2012**, *124*, 7617–7620.
[11] W. Piskorz, J. Gryboś, F. Zasada, P. Zapała, S. Cristol, J.-F. Paul, Z. Sojka, *J. Phys. Chem. C* **2012**, *116*, 19307–19320.
[12] a) J. Pinkas, I. Císařová, R. Gyepes, J. Kubišta, M. Horáček, K. Mach, *Organometallics* **2013**, *32*, 6306–6314; b) M. Manßen, L. L. Schafer, *Chem. Soc. Rev.* **2020**, *49*, 6947–6994; c) H. Helten, B. Dutta, J. R. Vance, M. E. Sloan, M. F. Haddow, S. Sproules, D. Collison, G. R. Whittell, G. C. Lloyd-Jones, I. Manners, *Angew. Chem. Int. Ed. Engl.* **2013**, *52*, 437–440.
[13] a) W. Kaim, *J. Am. Chem. Soc.* **1983**, 105, 707–713 ; b) T. Saito, H. Nishiyama, H. Tanahashi, K. Kawakita, H. Tsurugi, K. Mashima, *J. Am. Chem. Soc.* **2014**, *136*, 5161–5170; c) H. Tsurugi, K. Mashima, *Acc. Chem. Res.* **2019**, *52*, 769–779.
[14] H. M. Walborsky, *Acc. Chem. Res.* **1990**, *23*, 286–293.
[15] D. F. Evans, *J. Chem. Soc. (Resumed)* **1959**, 2003.
[16] a) S. B. Jones, J. L. Petersen, *J. Am. Chem. Soc.* **1983**, *105*, 5502–5503; b) E. Salvadori, M. Chiesa, A. Buonerba, A. Grassi, *Chem. Sci.* **2020**, *11*, 12436–12445; c) E. Samuel, P. Maillard, C. Giannotti, *J. Organomet. Chem.* **1977**, *142*, 289–298.
[17] H. C. Brown, R. G. Naik, B. Singaram, C. Pyun, *Organometallics* **1985**, *4*, 1925–1929.
[18] W. W. Lukens, R. A. Andersen, *Inorg. Chem.* **1995**, *34*, 3440–3443.
[19] a) M. González-Maupoey, V. Tabernero, T. Cuenca, *Coord. Chem. Rev.* **2009**, *253*, 1854–1881; b) J. Ho, D. W. Stephan, *Organometallics* **1992**,

11, 1014–1016; c) H. Brintzinger, J. E. Bercaw, *J. Am. Chem. Soc.* **1970**, *92*, 6182–6185; d) E. Samuel, *Inorg. Chem.* **1983**, *22*, 2967–2970.
[20] a) F. Bottomley, I. J. B. Lin, M. Mukaida, *J. Am. Chem. Soc.* **1980**, *102*, 5238–5242; b) A. F. R. Kilpatrick, F. G. N. Cloke, *Chem. Commun.* **2014**, *50*, 2769–2771; c) G. Fachinetti, C. Floriani, A. Chiesi-Villa, C. Guastini, *J. Am. Chem. Soc.* **1979**, *101*, 1767–1775.
[21] L. You, T. E. Hogen-Esch, Y. Zhu, J. Ling, Z. Shen, *Polymer* **2012**, *53*, 4112–4118.
[22] A. Aboulayt, C. Binet, J.-C. Lavalley, *J. Chem. Soc. Faraday Trans.* **1995**, *91*, 2913.
[23] C. Wu, L. Lin, J. Liu, J. Zhang, F. Zhang, T. Zhou, N. Rui, S. Yao, Y. Deng, F. Yang, W. Xu, J. Luo, Y. Zhao, B. Yan, X.-D. Wen, J. A. Rodriguez, D. Ma, *Nat. Commun.* **2020**, *11*, 5767.
[24] C. Imparato, M. Fantauzzi, C. Passiu, I. Rea, C. Ricca, U. Aschauer, F. Sannino, G. D'Errico, L. de Stefano, A. Rossi, A. Aronne, *J. Phys. Chem. C* **2019**, *123*, 11581–11590.
[25] C. Gionco, M. C. Paganini, E. Giamello, R. Burgess, C. Di Valentin, G. Pacchioni, *Chem. Mater.* **2013**, *25*, 2243–2253.
[26] J. Kim, B. B. Sarma, E. Andrés, N. Pfänder, P. Concepción, G. Prieto, *ACS Catal.* **2019**, *9*, 10409–10417.
[27] K. T. Jung, A. T. Bell, *Catal. Lett.* **2002**, *80*, 63–68.
[28] a) W. Piskorz, J. Gryboś, F. Zasada, S. Cristol, J.-F. Paul, A. Adamski, Z. Sojka, *J. Phys. Chem. C* **2011**, *115*, 24274–24286; b) W. Piskorz, J. Gryboś, F. Zasada, P. Zapała, S. Cristol, J.-F. Paul, Z. Sojka, *J. Phys. Chem. C* **2012**, *116*, 19307–19320.
[29] D. F. Shriver, M. A. Drezdzon, *The manipulation of air-sensitive compounds*, Wiley, New York, NY, **1986**.
[30] S. Stoll, A. Schweiger, *J. Magn. Reson.* **2006**, *178*, 42–55.
[31] G. A. Bain, J. F. Berry, *J. Chem. Educ.* **2008**, *85*, 532.
[32] K. Garrec, S. P. Fletcher, *Org. Lett.* **2016**, *18*, 3814–3817.
[33] G. te Velde, F. M. Bickelhaupt, E. J. Baerends, C. Fonseca Guerra, S. J. A. van Gisbergen, J. G. Snijders, T. Ziegler, *J. Comput. Chem.* **2001**, *22*, 931–967.
[34] a) J. P. Perdew, K. Burke, M. Ernzerhof, *Phys. Rev. Lett.* **1997**, *78*, 1396; b) J. P. Perdew, K. Burke, M. Ernzerhof, *Phys. Rev. Lett.* **1996**, *77*, 3865–3868; c) S. Grimme, S. Ehrlich, L. Goerigk, *J. Comput. Chem.* **2011**, *32*, 1456–1465; d) A. Schäfer, H. Horn, R. Ahlrichs, *J. Chem. Phys.* **1992**, *97*, 2571–2577.
[35] a) Y. Zhao, D. G. Truhlar, *Theor. Chim. Acta* **2008**, *120*, 215–241; b) D. Rappoport, F. Furche, *J. Chem. Phys.* **2010**, *133*, 134105.
[36] a) G. Henkelman, H. Jónsson, *J. Chem. Phys.* **1999**, *111*, 7010–7022; b) J. Kästner, P. Sherwood, *J. Chem. Phys.* **2008**, *128*, 14106.
[37] A. Klamt, G. Schüürmann, *J. Chem. Soc, Perkin Trans. 2* **1993**, 799–805.

Manuscript received: November 15, 2022
Revised manuscript received: February 14, 2023
Accepted manuscript online: February 14, 2023